Kondo-Dicke resonances in electronic transport through triple quantum dots

Piotr Trocha[1,*] and Józef Barnaś[1,2,†]

[1] *Department of Physics, Adam Mickiewicz University, 61-614 Poznań, Poland*
[2] *Institute of Molecular Physics, Polish Academy of Sciences, 60-179 Poznań, Poland*

(Dated: March 28, 2008)

Electronic transport through a triple quantum dot system, with only a single dot coupled directly to external leads, is considered theoretically. The model includes Coulomb correlations in the central dot, while such correlations in the two side-coupled dots are omitted. The infinite-U mean-field slave-boson approach is used to obtain basic transport characteristics in the Kondo regime. When tuning position of the side-coupled dots' levels, transition from *subradiant* to *superradiant* like mode (and *vice versa*) has been found in the spectral function, in analogy to the Dicke effect in atomic physics. Bias dependence of the differential conductance and zero frequency shot noise is also analysed.

PACS numbers:

I. INTRODUCTION

Kondo effect in electronic transport through quantum dots (QDs) strongly coupled to external leads is a many body phenomenon which occurs at temperatures T lower than the so-called Kondo temperature T_K, $T < T_K$. The Kondo temperature is characteristic of a particular system and depends on the corresponding parameters (energy of the dot level, coupling strength to external leads, Coulomb parameter). Spin fluctuations in the dot, generated by coupling of the dot to external leads, give rise to a narrow peak in the dot's density of states (DOS) at the Fermi level. This Kondo peak enhances transmission through the dot, and leads to the unitary limit of the linear conductance at zero temperature, where the conductance reaches $2e^2/h$. The Kondo peak in DOS also leads to the so-called zero-bias (Kondo) anomaly in the differential conductance.

The Kondo effect in electronic transport through single quantum dots was extensively studied in the last two decades, both theoretically[1,2,3,4,5,6,7,8,9] and experimentally[10,11]. Recently, the Kondo-assisted transport through double-dot systems in the T-shaped[12,13,14], parallel[14,15,16,17,18,19,20,21,22], and series[18,23,24,25,26,27,28] geometries also has been addressed. There are, however, only a few papers on the Kondo phenomenon in electronic transport through triple-dot structures[29,30,31,32,33,34,35]. Such complex dot systems are of current interest from both fundamental and application points of view. Especially the interference effects in electronic transport attract much attention, as the multi-dot systems offer a unique possibility to study fundamental phenomena which earlier were observed in solid state physics and/or quantum optics. By specific design and fabrication of QD systems, one can investigate for instance the Aharonov-Bohm oscillations[36], Fano resonance[37,38], and others.

Very recently, the Dicke effect, which is well known in atomic optics[39,40], has been predicted also for electronic transport through quantum systems[41,42,43,44,45,46,47,48]. The key feature of the Dicke resonance in optics is the presence of a strong and very narrow spontaneous emission line (in addition to much broader lines) of a collection of atoms which are separated by a distance smaller than the wavelength of the emitted light[39,40]. Generally, the narrow (broad) line is associated with a state which is weakly (strongly) coupled to the electromagnetic field, and such long-lived (short-lived) state is called *subradiant* (*superradiant*) mode. In this paper we consider another realization of the Dicke-like effect, i.e. the Kondo-Dicke resonances in electronic transport through a system of three coupled quantum dots, where two side-coupled dots are noninteracting (vanishing Coulomb parameter, $U = 0$), while the central dot is coupled to the leads and is in the deep Kondo regime. In addition, we also observe behavior of the Kondo peak in DOS, which resembles the transition from *subradiant* to *superradiant* mode (or *vice versa*) in the usual Dicke effect. The theoretical approach we use in this paper is based on the slave-boson technique in the mean-field approximation.

The paper is organized as follows. In section 2 we describe the model of a three-dot system, and present the corresponding Hamiltonian in the slave-boson formulation. The mean-field approach to the problem is described in section 3. Numerical results on the Kondo problem are shown and discussed in section 4 for symmetric and asymmetric systems. Final conclusions are given in section 5.

II. DESCRIPTION OF THE MODEL

In this paper we consider a system of three single-level quantum dots. The whole system is coupled to external leads as shown schematically in Fig.1. The two side dots, labelled as QD1 and QD3, are coupled to the central dot QD2 *via* a direct hopping term. The dot QD2, in turn, is additionally attached to external electron reservoirs (see Fig.1). Moreover, the central dot is assumed to be in the Kondo regime, while the side dots are beyond the Kondo regime (for simplicity they are assumed to be noninteracting, $U = 0$). The system under consideration can be modelled by the Anderson impurity-like Hamiltonian of

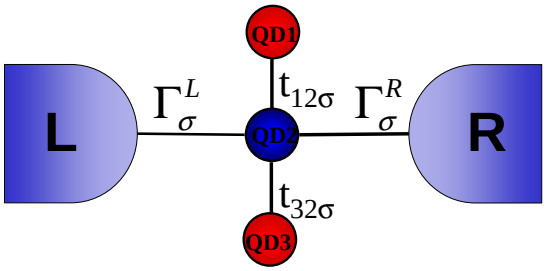

FIG. 1: Schematic picture of the quantum dot system coupled to external leads. Γ_σ^α ($\alpha = L, R$) describe coupling of the dot QD2 to the external leads, whereas $t_{j2\sigma}$ is the hopping parameter between the dot QD2 and the j-th dot, $j = 1, 3$

the following form:

$$\hat{H} = \sum_{\mathbf{k}\alpha\sigma} \varepsilon_{\mathbf{k}\alpha\sigma} c^\dagger_{\mathbf{k}\alpha\sigma} c_{\mathbf{k}\alpha\sigma} + \sum_{i\sigma} \epsilon_{i\sigma} d^\dagger_{i\sigma} d_{i\sigma} + U n_{2\sigma} n_{2\bar{\sigma}} + \sum_{j(=1,3)} \sum_\sigma (t_{j2\sigma} d^\dagger_{2\sigma} d_{j\sigma} + \text{h.c.}) + \sum_{\mathbf{k}\alpha} \sum_\sigma (V^\alpha_{\mathbf{k}\sigma} c^\dagger_{\mathbf{k}\alpha\sigma} d_{2\sigma} + \text{h.c.}). \quad (1)$$

The first term describes the left ($\alpha = L$) and right ($\alpha = R$) electrodes in the non-interacting quasi-particle approximation, with $c^\dagger_{\mathbf{k}\alpha\sigma}$ ($c_{\mathbf{k}\alpha\sigma}$) being the creation (annihilation) operator of an electron with the wave vector $\mathbf{k}$ and spin σ in the lead α, and with $\varepsilon_{\mathbf{k}\alpha\sigma}$ denoting the corresponding single-particle energy.

The next three terms of the Hamiltonian describe the system of three coupled quantum dots. Here, $\epsilon_{i\sigma}$ is the energy of the discrete level in the i-th dot ($i = 1, 2, 3$), while $t_{j2\sigma}$ denotes the hopping parameter between the j-th dot ($j = 1, 3$) and the dot QD2. Both $\epsilon_{i\sigma}$ and $t_{j2\sigma}$ can be spin dependent in a general case. Furthermore, the term with U describes the intra-dot Coulomb interactions in the dot QD2, with U denoting the corresponding Coulomb integral. The inter-dot Coulomb repulsion, similarly as the intra-dot Coulomb interaction for the dots QD1 and QD3, is assumed to be small and therefore neglected.

The last term of the system's Hamiltonian describes electron tunnelling from the leads to the dot QD2 (or *vice versa*), with $V^\alpha_{\mathbf{k}\sigma}$ denoting the relevant matrix elements ($\alpha = L, R$). Coupling of the dot QD2 to external leads can be parameterized in terms of $\Gamma^\alpha_\sigma(\varepsilon) = \pi \sum_{\mathbf{k}} V^\alpha_{\mathbf{k}\sigma} V^{\alpha *}_{\mathbf{k}\sigma} \delta(\varepsilon - \epsilon_{\mathbf{k}\alpha\sigma})$. We assume that $\Gamma^\alpha_\sigma(\varepsilon)$ is constant within the electron band of the leads, $\Gamma^\alpha_\sigma(\varepsilon) = \Gamma^\alpha_\sigma =$ const for $\varepsilon \in \langle -D, D \rangle$, and $\Gamma^\alpha_\sigma(\varepsilon) = 0$ otherwise. Here, $2D$ denotes the electron band width.

The following considerations are restricted to the limit of infinite intra-dot Coulomb parameter for the dot QD2, $U \to \infty$, so the double occupancy on the central dot is forbidden (only one electron can reside in the central dot). This assumption allows us to employ the infinite-U slave-boson mean-field (SBMF) approach[49] to analyze transport properties. However, one should bear in mind that the SBMF theory is valid only for low bias at zero temperature.

In the slave-boson approach, one introduces a set of auxiliary operators for the central dot. The dot's creation (annihilation) operator $d^\dagger_{2\sigma}$ ($d_{2\sigma}$) is then replaced with $f^\dagger_{2\sigma} b_2$ ($b^\dagger_2 f_{2\sigma}$). Here, b_2 ($f_{2\sigma}$) is the slave-boson (pseudofermion) annihilation operator for an empty (singly occupied with a spin-σ electron) state of the dot QD2. To eliminate non-physical states, the following constraint has to be imposed on the new quasi-particles,

$$\hat{Q} = \sum_\sigma f^\dagger_{2\sigma} f_{2\sigma} + b^\dagger_2 b_2 = 1. \quad (2)$$

Equation (2) is a completeness relation of the Hilbert space for the central dot. Accordingly, the Hamiltonian (1) can be replaced by an effective Hamiltonian, expressed in terms of the auxiliary boson b_2 and pseudofermion $f_{2\sigma}$ operators as

$$\tilde{H} = \sum_{\mathbf{k}\alpha\sigma} \varepsilon_{\mathbf{k}\alpha\sigma} c^\dagger_{\mathbf{k}\alpha\sigma} c_{\mathbf{k}\alpha\sigma} + \sum_\sigma \left(\epsilon_{1\sigma} d^\dagger_{1\sigma} d_{1\sigma} + \epsilon_{3\sigma} d^\dagger_{3\sigma} d_{3\sigma} \right) + \sum_\sigma \epsilon_{2\sigma} f^\dagger_{2\sigma} f_{2\sigma} + \frac{1}{\sqrt{N}} \sum_{j(=1,3)} \sum_\sigma (t_{j2\sigma} f^\dagger_{2\sigma} b_2 d_{j\sigma} + \text{h.c.}) + \frac{1}{\sqrt{N}} \sum_{\mathbf{k}\alpha} \sum_\sigma (V^\alpha_{\mathbf{k}\sigma} c^\dagger_{\mathbf{k}\alpha\sigma} b^\dagger_2 f_{2\sigma} + \text{h.c.}) + \lambda \left(\sum_\sigma f^\dagger_{2\sigma} f_{2\sigma} + b^\dagger_2 b_2 - 1 \right). \quad (3)$$

The last term with the Lagrange multiplier λ has been introduced to incorporate the constraint for QD2, given by Eq.(2), which prevents double occupancy of the central dot. Apart from this, $N(= 2)$ in Eq.(3) stands for the spin-degeneracy of the QD2. One can check that the number operator $\hat{Q}$ (see Eq.(2)) commutes with this new Hamiltonian, so the total particle number of f-electrons and slave bosons is conserved.

III. MEAN FIELD APPROACH

The mean field approximation (MFA) adopted to the slave-boson method relies on replacing the boson field b_2 by its expectation value. Thus, in the lowest order (in the $1/N$ expansion), the slave-boson operator is substituted by a real and independent of time c number, $b_2(t)/\sqrt{N} \to \langle b_2(t) \rangle / \sqrt{N} \equiv \tilde{b}_2$. This approximation neglects fluctuations around the average value $\langle b_2(t) \rangle$ of the slave boson operator, but takes into account spin fluctuations (Kondo regime) – exactly at $T = 0K$ and in the limit of $N \to \infty$. On the other hand, one should bear in mind that MFA cannot be applied in the mixed-valence regime, where strong charge fluctuations take place. That is why the MFA approach restricts our considerations to the low bias regime ($eV \ll |\epsilon_2|$). Introducing the following renormalized parameters $\tilde{t}_{j2\sigma} = \tilde{b}_2 t_{j2\sigma}$,

$\tilde{V}^{\alpha}_{\mathbf{k}\sigma} = V^{\alpha}_{\mathbf{k}\sigma}\tilde{b}_2$ and $\tilde{\epsilon}_{2\sigma} = \epsilon_{2\sigma} + \lambda$, the effective MFA Hamiltonian can be rewritten as

$$\tilde{H}^{MFA} = \sum_{\mathbf{k}\alpha\sigma} \varepsilon_{\mathbf{k}\alpha\sigma} c^{\dagger}_{\mathbf{k}\alpha\sigma} c_{\mathbf{k}\alpha\sigma} + \sum_{i=1,3}\sum_{\sigma} \epsilon_{i\sigma} d^{\dagger}_{i\sigma} d_{i\sigma} + \sum_{\sigma} \tilde{\epsilon}_{2\sigma} f^{\dagger}_{2\sigma} f_{2\sigma} + \sum_{j(=1,3)}\sum_{\sigma} (\tilde{t}_{j2\sigma} f^{\dagger}_{2\sigma} d_{j\sigma} + \text{h.c.}) + \sum_{\mathbf{k}\alpha}\sum_{\sigma} (\tilde{V}^{\alpha}_{\mathbf{k}\sigma} c^{\dagger}_{\mathbf{k}\alpha\sigma} f_{2\sigma} + \text{h.c.}) + \lambda\left(N\tilde{b}^2 - 1\right). \quad (4)$$

One needs now to find the unknown parameters $\tilde{b}_2$ and λ. These can be determined from the constraint imposed on the slave bosons (Eq.(2)), and from the equation of motion for the slave boson operators. As a result, one finds two equations,

$$\frac{1}{N}\sum_{\sigma}\langle f^{\dagger}_{2\sigma} f_{2\sigma}\rangle + \tilde{b}_2 = \frac{1}{N}, \quad (5)$$

$$\sum_{j=1,3}\sum_{\sigma} \tilde{t}^{*}_{j2\sigma}\langle d^{\dagger}_{j\sigma} f_{2\sigma}\rangle + \sum_{\mathbf{k}\alpha\sigma} \tilde{V}^{\alpha}_{\mathbf{k}\sigma}\langle c^{\dagger}_{\mathbf{k}\alpha\sigma} f_{2\sigma}\rangle + N\lambda\tilde{b}_2 = 0. \quad (6)$$

There is also another way to obtain the above equations. The free parameters $\tilde{b}_2$ and λ can be determined by minimizing the ground state energy of the effective MFA Hamiltonian with respect to these parameters. Application of the Hellmann-Feynman theorem to the Hamiltonian (4), together with the conditions for minimal energy $(\partial\langle\tilde{H}^{MFA}\rangle/\partial\tilde{b}) = 0 = (\partial\langle\tilde{H}^{MFA}\rangle/\partial\lambda)$, gives a set of self-consistent equations. These equations in the Fourier space read

$$\tilde{b}_2 - i\sum_{\sigma}\int \frac{d\varepsilon}{2\pi N}\langle\langle f_{2\sigma}|f^{\dagger}_{2\sigma}\rangle\rangle^{<}_{\varepsilon} = \frac{1}{N}, \quad (7)$$

$$-i\sum_{j=1,3}\sum_{\sigma}\tilde{t}^{*}_{j2\sigma}\int\frac{d\varepsilon}{2\pi}\langle\langle f_{2\sigma}|d^{\dagger}_{j\sigma}\rangle\rangle^{<}_{\varepsilon} - i\sum_{\mathbf{k}\alpha\sigma}\tilde{V}^{\alpha}_{\mathbf{k}\sigma}\int\frac{d\varepsilon}{2\pi}\langle\langle f_{2\sigma}|c^{\dagger}_{\mathbf{k}\alpha\sigma}\rangle\rangle^{<}_{\varepsilon} + N\lambda\tilde{b}_2 = 0, \quad (8)$$

where $\langle\langle f_{2\sigma}|d^{\dagger}_{j\sigma}\rangle\rangle^{<}_{\varepsilon}$ and $\langle\langle f_{2\sigma}|c^{\dagger}_{\mathbf{k}\alpha\sigma}\rangle\rangle^{<}_{\varepsilon}$ are the Fourier transforms of the lesser Green functions; the former being defined as $G^{<}_{2j}(t,t') \equiv \langle\langle f_{2\sigma}(t)|d^{\dagger}_{j\sigma}(t')\rangle\rangle^{<} = i\langle d^{\dagger}_{j\sigma}(t') f_{2\sigma}(t)\rangle$ and a similar definition also holds for $\langle\langle f_{2\sigma}(t)|c^{\dagger}_{\mathbf{k}\alpha\sigma}(t')\rangle\rangle^{<}$.

To rewrite Eq.(8) in a different form, we write first the equation of motion for $f_{2\sigma}(t)$. Then, we multiply this equation by $f^{\dagger}_{2\sigma}(t')$ and take the thermal average. Upon expressing the obtained equation in terms of the lesser Green functions, and taking its hermitian conjugation, one finds

$$(\varepsilon - \tilde{\epsilon}_{2\sigma})\langle\langle f_{2\sigma}|f^{\dagger}_{2\sigma}\rangle\rangle^{<}_{\varepsilon} = \sum_{j=1,3}\sum_{\sigma}\tilde{t}^{*}_{j2\sigma}\langle\langle f_{2\sigma}|d^{\dagger}_{j\sigma}\rangle\rangle^{<}_{\varepsilon} + \sum_{\mathbf{k}\alpha\sigma}\tilde{V}^{\alpha}_{\mathbf{k}\sigma}\langle\langle f_{2\sigma}|c^{\dagger}_{\mathbf{k}\alpha\sigma}\rangle\rangle^{<}_{\varepsilon}. \quad (9)$$

When substituting Eq.(9) into Eq.(8), one finally arrives at the equation

$$-i\sum_{\sigma}\int\frac{d\varepsilon}{2\pi}(\varepsilon - \tilde{\epsilon}_{2\sigma})\langle\langle f_{2\sigma}|f^{\dagger}_{2\sigma}\rangle\rangle^{<}_{\varepsilon} + N\lambda\tilde{b}_2 = 0. \quad (10)$$

Formulas (7) and (10) are our final equations for the unknown parameters. To solve them one still needs to determine the lesser Green function $\langle\langle f_{2\sigma}|f^{\dagger}_{2\sigma}\rangle\rangle^{<}_{\varepsilon}$. This can be derived from the corresponding equation of motion. Similarly, the equation of motion can also be used to derive the retarded Green function (which is also required in our calculations). As a result one finds

$$G^{r}_{22\sigma}(\varepsilon) = \frac{1}{\varepsilon - \tilde{\epsilon}_{2\sigma} + i\tilde{\Gamma}_{\sigma} - \frac{\tilde{t}^2_{32\sigma}}{\varepsilon-\epsilon_{3\sigma}} - \frac{\tilde{t}^2_{12\sigma}}{\varepsilon-\epsilon_{1\sigma}}}, \quad (11)$$

$$G^{<}_{22\sigma}(\varepsilon) = \frac{2i[f_L(\varepsilon)\tilde{\Gamma}^{L}_{\sigma} + f_R(\varepsilon)\tilde{\Gamma}^{R}_{\sigma}]}{\left|\varepsilon - \tilde{\epsilon}_{2\sigma} + i\tilde{\Gamma}_{\sigma} - \frac{\tilde{t}^2_{32\sigma}}{\varepsilon-\epsilon_{3\sigma}} - \frac{\tilde{t}^2_{12\sigma}}{\varepsilon-\epsilon_{1\sigma}}\right|^2}, \quad (12)$$

where $f_{\alpha}(\varepsilon)$ is the Fermi-Dirac distribution function in lead α, $\tilde{\Gamma}^{\alpha}_{\sigma} = \tilde{b}^2_2\Gamma^{\alpha}_{\sigma}$ and $\tilde{\Gamma}_{\sigma} = \tilde{\Gamma}^{L}_{\sigma} + \tilde{\Gamma}^{R}_{\sigma}$ are the renormalized parameters describing coupling of the dot QD2 to external leads.

Electric current J flowing through the system can be determined from the formula

$$J = \frac{e}{h}\sum_{\sigma}\int d\varepsilon[f_L(\varepsilon) - f_R(\varepsilon)]T_{\sigma}(\varepsilon), \quad (13)$$

where $T_{\sigma}(\varepsilon) = 4G^{a}_{22\sigma}\tilde{\Gamma}^{R}_{\sigma}G^{r}_{22\sigma}\tilde{\Gamma}^{L}_{\sigma}$ is the transmission probability. It is worth noting that the above current formula is similar to that used for noninteracting QD systems. In our case, however, the transmission probability depends on the renormalized parameters $\tilde{\Gamma}^{\alpha}_{\sigma}$, $\tilde{\epsilon}_{2\sigma}$ and $\tilde{t}_{j2\sigma}$, which depend on the gate and transport voltages. At $T = 0$K, the current and linear conductance are given by the formula

$$J_0 = \frac{e}{h}\sum_{\sigma}\int_{-eV/2}^{eV/2} d\varepsilon\; T_{\sigma}(\varepsilon), \quad (14)$$

and

$$G_{V\to 0} = \lim_{V\to 0}\frac{dJ}{dV} = \frac{e^2}{h}\sum_{\sigma}T_{\sigma}(\varepsilon = 0). \quad (15)$$

IV. NUMERICAL RESULTS

In numerical calculations we assume that the dot levels and the hoping parameters are independent of electron spin, $\epsilon_{i\sigma} = \epsilon_i$ (for $i = 1, 2, 3$), $t_{j2\sigma} = t_{j2}$ for $j = 1, 3$, and $\Gamma^{\alpha}_{\sigma} = \Gamma^{\alpha}$ (for $\alpha = L, R$). The energy levels ϵ_i are measured from the Fermi level of the leads in equilibrium ($\mu_L = \mu_R = 0$). In the following we set the bare level

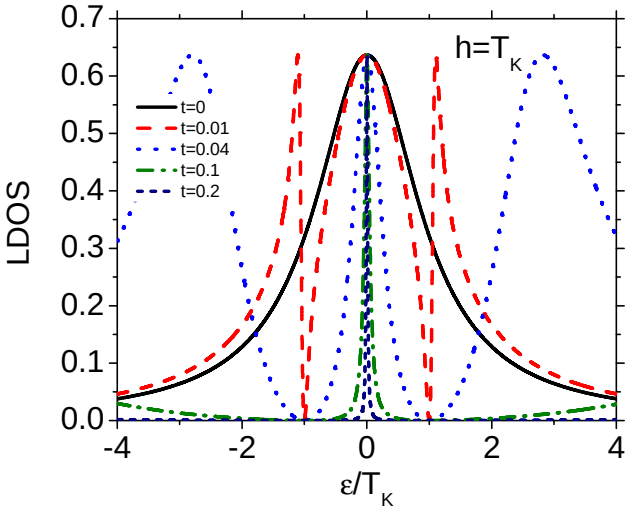

FIG. 2: Local density of states for the dot QD2, calculated for indicated values (in the units of Γ) of the interdot coupling strength $t_{12} = t_{32} = t$, and for $\epsilon_1 = -\epsilon_3 \equiv h = T_K = 0.001\Gamma$.

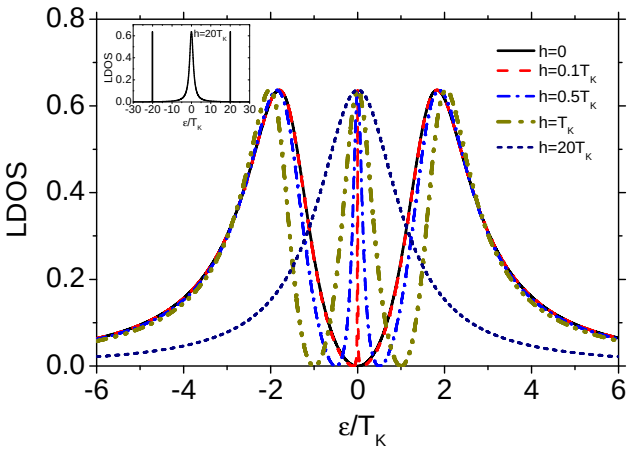

FIG. 3: Local density of states for the dot QD2 calculated for indicated values of h ($h = \epsilon_1 = -\epsilon_3$), and for the interdot coupling $t_{12} = t_{32} = t = 0.03\Gamma$.

of the dot QD2 at $\epsilon_2 = -3.5\Gamma$, and the bandwidth is assumed to be $D = 60\Gamma$. In this paper all the energy quantities will be expressed in the units of Γ ($\Gamma = \Gamma^L + \Gamma^R$). The energy levels ϵ_1 and ϵ_3 can be tuned by applying gate voltages to QD1 and QD3. Taking into account the above parameters, the Kondo temperature T_K of the central dot for $t_{12} = t_{32} = 0$ can be estimated to be $T_K = 10^{-3}\Gamma$ ($k_B = 1$).

A. Density of states

We start from the local density of states (LDOS) at equilibrium, D_2, for the central dot QD2, which can be calculated from the formula

$$D_2 = -\frac{\tilde{b}_2^2}{\pi} \sum_\sigma \Im \left[G^r_{22\sigma}(\varepsilon) \right], \tag{16}$$

where $\Im[A]$ denotes the imaginary part of A.

To understand basic features of the LDOS D_2 in the Kondo regime and the influence of side-coupled dots, we consider first the situation when the dot levels are fixed while the coupling between the dots can be changed. The corresponding LDOS is shown in Fig.2 for several values of $t_{12} = t_{32} \equiv t$. Assume first that the central dot is detached from the two dots QD1 and QD3, $t = 0$ (solid line in Fig.2). The peak at the Fermi level in D_2 reveals then the usual Kondo phenomenon in a single dot, which leads to the Kondo anomaly in transport through the dot (to be discussed later). If now one additional and noninteracting dot is attached to the Kondo dot *via* a hopping term, the shape of the Kondo peak is changed due to the interference effects (not shown in Fig.2). As it has been shown by Wu *et al*[12], the DOS can be then decomposed into a Breit-Wigner and a Fano line shape. Assume now that another non-interacting dot has been connected to the Kondo dot, as in the case shown in Fig.1. Let the bare levels of the side-coupled dots are fixed at T_K and $-T_K$, respectively. When the interdot coupling strength t is nonzero, two additional asymmetric satellite peaks emerge in LDOS D_2. As shown in Fig.2, these peaks move away from the central peak as t increases. At the same time, the widths of the satellite peaks increase, while the central peak becomes narrower.

In Fig.3 the LDOS for the dot QD2 is shown for different energy levels of the side-coupled dots, while coupling of these dots to the central dot is fixed, $t_{12} = t_{32} = t = 0.03\Gamma$. It has been assumed there that the energy levels of the dots QD1 and QD3 are located symmetrically with respect to the Fermi level at equilibrium, $\epsilon_1 = h$ and $\epsilon_3 = -h$. For a nonzero h, the LDOS reveals three well defined peaks. The central peak (the main Kondo peak) is located at the Fermi level of the leads, while the other two satellite peaks are roughly at $\pm\sqrt{h^2 + 2\tilde{t}^2}$. When $h << t$, position of these satellite peaks is only weakly dependent on h. Between the maxima, the LDOS goes to zero at $\epsilon = \pm h$. The width of central peak becomes narrower and narrower with decreasing h, and the peak has almost δ-like shape for very small values of h, $h \ll t$. This means that the Kondo state associated with this maximum becomes then more and more localized at the Fermi level. In analogy to the Dicke effect, which is well known in optics, the narrow central peak in LDOS may be considered as a long-lived (*subradiant*) state, whereas the other two peaks as corresponding to short-lived (*superradiant*) states. It is interesting to note that one can observe transition from *subradiant* to *superradiant* mode (and *vice versa*) by tuning separation of the side-coupled dots' levels from the Fermi level, e.g. by gate voltages. Thus, a particular state, for example the one at the Fermi level, is *subradiant*-like for small values of h ($h \ll t$), and

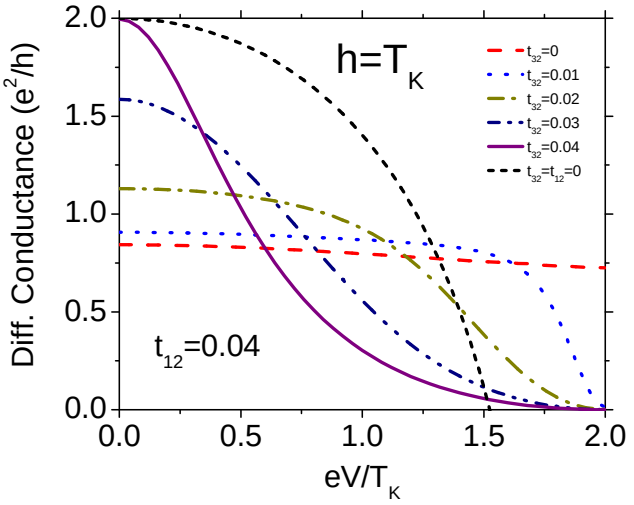

FIG. 4: Differential conductance as a function of the applied bias voltage for indicated values of the interdot couplings (measured in the units of Γ).

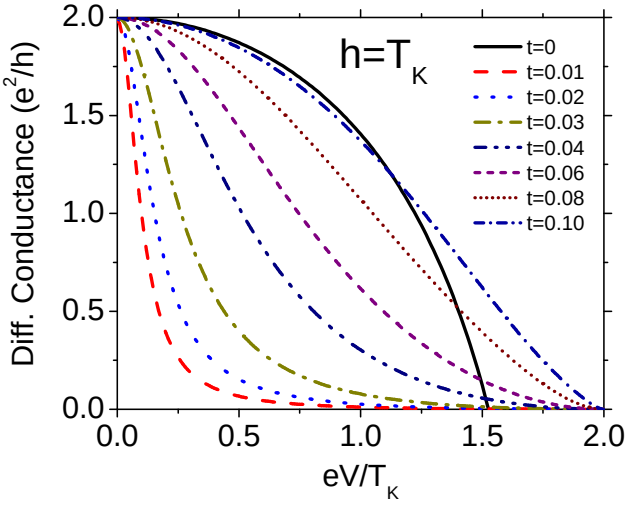

FIG. 5: Differential conductance as a function of the bias voltage for indicated values of the interdot couplings $t = t_{12} = t_{32}$ (measured in the units of Γ).

superradiant-like for large values of h ($h \gg t$). When the energy levels of the side-coupled dots coincide with the Fermi level, $h = 0$, the Kondo peak (central peak) in LDOS is suppressed and disappears.

For large values of the side dots' level separation ($h \gg t$), the satellite peaks are narrow, while the central peak is then relatively broad. This situation is qualitatively similar to that observed in Ref.[50]. However, the width of the central peak is now a complex non-monotonic function of the level separation h (due to self-consistent parameters $\tilde{b}_2$, λ). The width of the peak increases for small values of h achieving a maximum and then decreases very slowly (even for large values of h). Moreover, in the nonlinear response regime, when a nonzero bias voltage is applied to the system, the width of the central peak is further suppressed, especially for large h. Position of the maximum moves to smaller values of h as bias voltage increases. Another new feature is a broad range of very small LDOS between the central maximum and the satellite peaks for larger values of h.

To summarize this section we conclude that the width of the Kondo peak in LDOS can be changed by tuning both the level position of side dots and the inter dot coupling strength. Such systems give us an opportunity to study cross-over from the *subradiant* to *superradiant* mode, and *vice versa*.

B. Differential conductance

Now we consider nonlinear differential conductance dJ/dV. In Fig.4 we show differential conductance as a function of the applied voltage for the case when the dot QD1 is coupled to the Kondo dot with a constant strength, $t_{12} = 0.04\Gamma$, while the coupling strength of

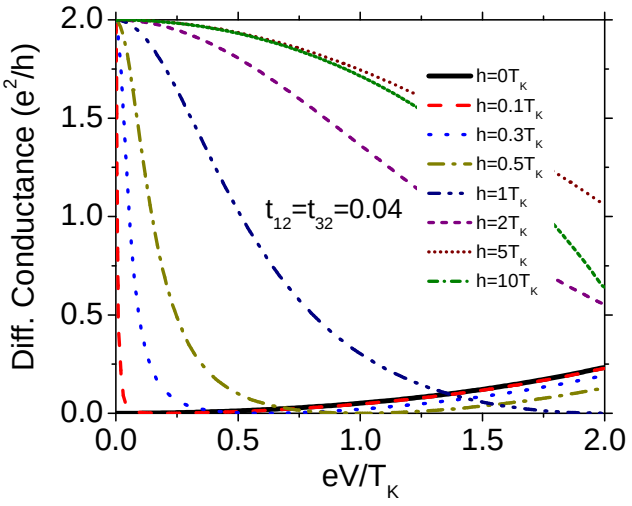

FIG. 6: Differential conductance as a function of the bias voltage for indicated value od the coupling strengths (measured in the units of Γ), and indicated energy levels of the side-coupled dots, $\epsilon_1 = -\epsilon_3 = h$.

the dot QD3 is gradually switched on. For comparison we have also shown there the curve for the Kondo dot totally decoupled from both side dots, $t_{12} = t_{32} = 0$. Owing to the Kondo resonance, the unitary limit of the conductance is then reached for zero bias limit. This is well know behavior of transport through a single Kondo dot. Let us now turn on the coupling of the Kondo dot to one of the side dots, say to the dot QD1. The zero bias anomaly becomes then suppressed as a consequence of the interplay between the Fano interference and the Kondo effect[12]. For a sufficiently large t_{12}, the zero bias anomaly may even disappear. However, the situation becomes more complex when the second side dot (QD3)

is attached to the Kondo dot and starts to play a role in transport. With increasing coupling strength t_{32} of the dot QD3 to the dot QD2, one observes revival of the zero bias anomaly peak, which for $t_{32} = t_{12}$ reaches unitary limit for zero bias. Interplay of the Dicke and Kondo resonances leads, however, to a faster decrease of the conductance at small voltages, and slower at higher voltages. As a consequence, a tail in the conductance survives at higher voltages, where the conductance of the Kondo dot detached from the side dots already disappears. This behavior is a consequence of the narrowing of the central Kondo peak in LDOS and the occurrence of two satellite peaks (see discussion in the previous subsection). This behavior is clearly seen in Fig. 5, where the bias dependence of the differential conductance is shown for several values of the inter-dot coupling parameters, $t_{32} = t_{12} = t$. The zero bias conductance in such a symmetrical case does not depend on the value of t, which reflects the LDOS behavior (see Fig.2).

Similar behavior also occurs when the coupling strength $t_{12} = t_{32} \equiv t$ are fixed while the level separation of the side-coupled dots is changed (see Fig.6). For large values of h the conductance decreases with increasing bias monotonically. However, for small values of h the differential conductance is a nonmonotonic function of the applied bias voltage. It falls down rapidly in the region of small bias voltages achieving a minimum value at some voltage, and then rises again. These features are quite reasonable because the satellite peaks move away from the central peak as h increases. Thus, for large values of h the satellite peaks do not contribute to electronic transport. For a small h, however, the satellite peaks enter the transport window and contribute to current, leading to an increase in the conductance above a certain bias voltage. It is worth to note, that the zero bias anomaly for $h = 0$ is totally suppressed and the differential conductance slowly rises as the bias voltage is applied. This suppression is a consequence of the suppression of the Kondo peak in DOS due to the interplay of the Dicke and Kondo resonances.

C. Shot noise

The only nonzero contribution to the noise in electronic transport at zero temperature, $T = 0K$, is the shot noise, while the thermal noise is then totally suppressed. The quadratic form of the MFA Hamiltonian allows us to express the zero frequency shot noise in the form,

$$S = \frac{2e^2}{h} \int_{-eV/2}^{eV/2} d\epsilon T_\sigma(\epsilon)[1 - T_\sigma(\epsilon)]. \qquad (17)$$

Deviation of the shot noise S from the Poisson value, $S_P = 2eJ$, is usually characterized by the Fano factor $\gamma = S/2eJ$, which for the Poissonian noise is exactly equal to 1.

In Fig. 7, the bias dependence of the Fano factor is displayed for different interdot coupling parameters t_{32},

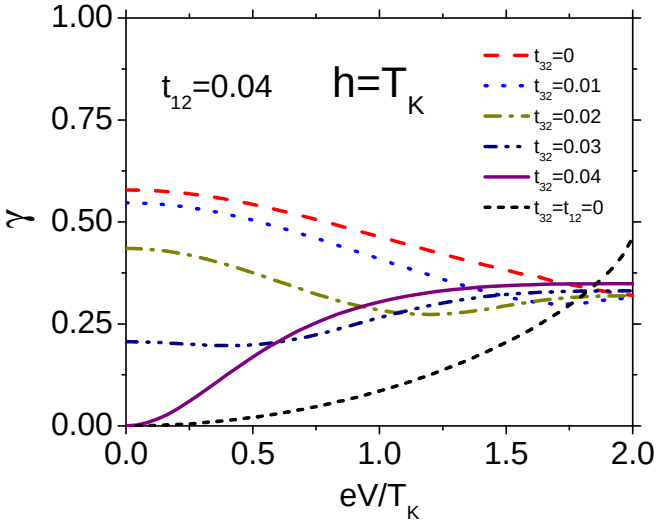

FIG. 7: Fano factor as a function of the applied bias voltage for indicated values of the interdot couplings (measured in the units of Γ).

whereas the parameter t_{12} is fixed at 0.04Γ. For the T-shape geometry (one side dot is decoupled from the central dot QD2, $t_{32} = 0$), the Fano interference plays a significant role in transport processes, and – as discussed above – leads to suppression of the zero bias anomaly below the unitary limit. This is also manifested in the shot noise characteristics. The zero bias limit of the Fano factor is larger than zero, and this behavior is a result of the weakening of the Kondo peak at the Fermi level due to the Fano interference. With increasing t_{12}, but still having $t_{32} = 0$, the Fano interference outweighs the Kondo effect and the Fano factor γ tends to unitary limit (shot noise tends to the Poissonian value). When coupling of the dot QD3 to the dot QD2 is turned on, the zero bias Fano factor drops and finally for a symmetric system, $t_{12} = t_{32}$, reaches zero as for the single quantum dot. As a result, the system is ideally transparent for electrons at the Fermi energy $\mu = 0$ (at the equilibrium).

Figure 8 shows the Fano factor as a function of the applied voltage for various inter-dot couplings, $t_{32} = t_{12} = t$. Applied bias voltage partially suppresses the Kondo effect, which results in the growth of the Fano factor. This growth is faster for smaller values of t.

When the levels of the side coupled dots are located at the Fermi level ($h = 0$), the zero bias Fano factor achieves the Poissonian value and then slowly falls down with increasing bias voltage (see Fig.9). In contrary, the zero bias limit of the Fano factor for a nonzero level separation of the side-coupled dots is zero and tends to the Poissonian limit with increasing bias voltage. One can then note a sudden increase of the Fano factor for a small value of the level separation, $h < T_K$, while for $h > T_K$ the Fano factor remains small over a wider range of the bias voltage before it grows to the Poisson limit.

In Fig.10 the Fano factor γ is plotted as a function

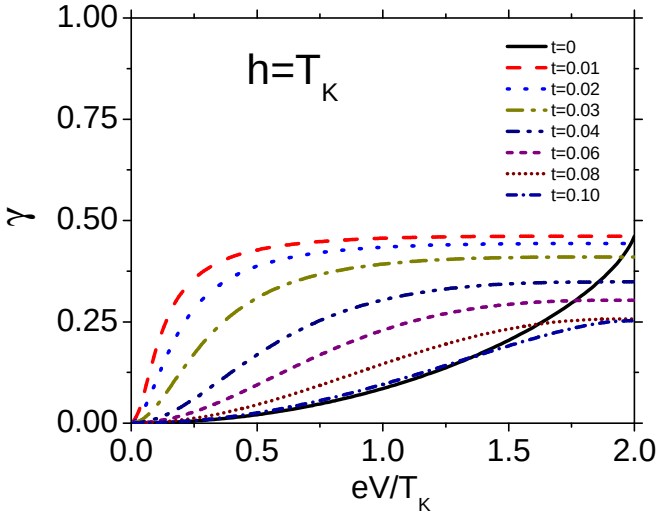

FIG. 8: Fano factor as a function of the bias voltage for various values of the interdot couplings $t = t_{12} = t_{32}$ (measured in the units of Γ).

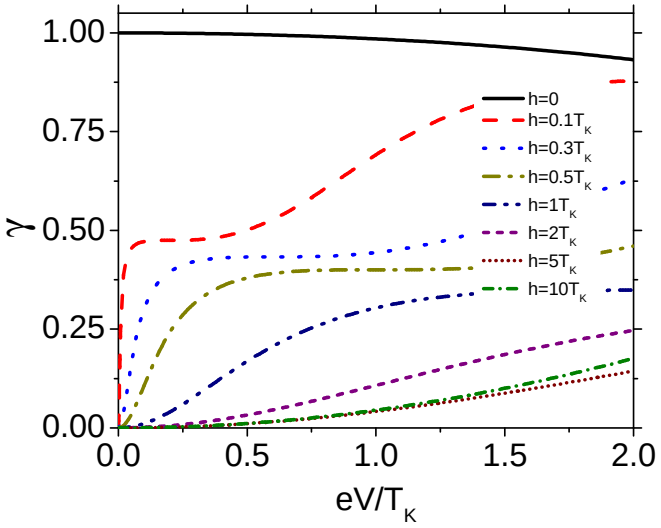

FIG. 9: Fano factor as a function of the bias voltage for indicated side-coupled dots' levels; $\epsilon_1 = h$, $\epsilon_3 = -h$, and for $t_{12} = t_{31} = 0.04\Gamma$.

of t for a fixed bias voltage $eV = T_K$, and for different positions of the side-coupled dots' levels ($\epsilon_1 = h$, $\epsilon_3 = -h$). When the bare levels of side-coupled dots are in the transport window, the Fano factor is then significantly affected by the interdot coupling. For a very small value of h, the Fano factor grows rapidly from a small value at zero interdot coupling to its maximum values, and then falls down to half of the Poissonian value at sufficiently strong couplings. It is worth to note that the Fano factor does not reach the Poissonian limit for any h, except the case of $h = 0$. In turn, for $h >> T_K$ the Fano factor γ is less sensitive to the interdot coupling strength. The

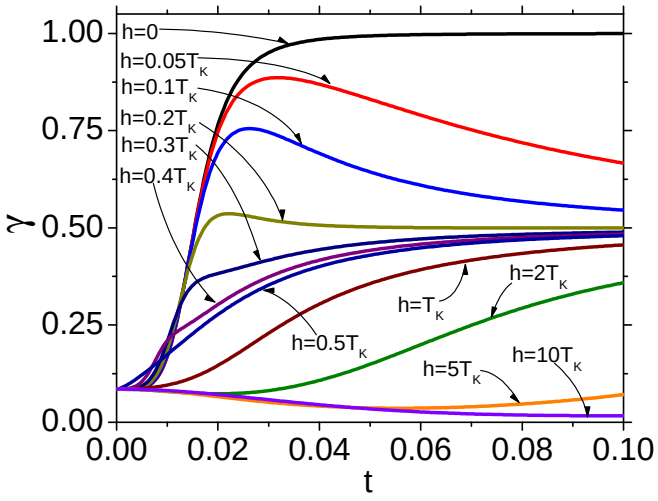

FIG. 10: Fano factor as a function of the interdot coupling strength t for different values of h; $\epsilon_1 = h$, $\epsilon_3 = -h$. The bias is fixed at $eV = T_K$.

central peak in the LDOS is then very broad and gives a large contribution to the differential conductance. On can also note that for a large value of h, γ remains small in a wider range of the interdot coupling before it rises to half of the Poisson value. Contrary to the case of small h, one can now see a minimum in the the Fano factor (for a finite bias). Thus, the Kondo-assisted transport is optimized for $t = t_{min}$.

V. SUMMARY AND CONCLUSIONS

In this paper we have considered the effects due to interplay of the Kondo and Dicke resonances in electronic transport through a three-dot system. One of the dot (that attached to the leads) was in the Kondo regime, while the two side dots were out of the Kondo regime. Using the method based on the slave boson mean field approximation we have calculated local density of states, differential conductance, and shot noise. The results clearly show that the side dots strongly modify the transport characteristics.

The Kondo peak in the local density of states of the central dot becomes narrower due to the interplay of the Kondo and Dicke effects. The Kondo peak is even totally suppressed when the bare energy levels of the side dots are equal and located at the Fermi level. This leads to suppression of the zero bias Kondo peak in the differential conductance. The interplay of the Kondo an Dicke resonances has also a significant impact on the shot noise characteristics.

Acknowledgments

This work, as part of the European Science Foundation EUROCORES Programme SPINTRA, was supported by funds from the Ministry of Science and Higher Education as a research project in years 2006-2009 and the EC Sixth Framework Programme, under Contract N. ERAS-CT-2003-980409.

* Electronic address: piotrtroch@o2.pl
† Electronic address: barnas@amu.edu.pl

[1] L. I. Glazman and M. E. Raikh, JETP Lett. **47**, 452 (1988); T. K. Ng and P. A. Lee, Phys. Rev. Lett. **61**, 1768 (1988).
[2] Y. Meir, N. S. Wingreen, and P. A. Lee, Phys. Lett. **66**, 3048 (1991).
[3] Y. Meir, N. S. Wingreen, and P. A. Lee, Phys. Lett. **70**, 2601 (1993).
[4] P. Nordlander, M. Pustilnik, Y. Meir, N. S. Wingreen, D. C. Langreth, Phys. Lett. **83**, 808 (1999).
[5] Y. Meir and A. Golub, Phys. Lett. **88**, 116802 (2002).
[6] K. Kang and B. I. Min, Phys. Rev. B **52**, 10689 (1995).
[7] B. Dong and X. L. Lei, Phys. Rev. B **53**, 235306 (2001).
[8] R. Świrkowicz, M. Wilczyński, M. Wawrzyniak, and J. Barnaś, Phys. Rev. B **73**, 193312 (2006).
[9] R. Świrkowicz, M. Wilczyński, and J. Barnaś, J. Phys.: Condens. Matter **18**, 2291 (2006).
[10] S. M. Cronenwett et al., Science **281**, 540 (1998); S. Sasaki, S. De Franceschi, J. M. Elzerman, W. G. van der Wiel, M. Eto, S. Tarucha, and L. P. Kouvenhoven, Nature (London) **405**, 764 (2000).
[11] J. Gores, D. Goldhaber-Gordon, S. Heemeyer, M. A. Kastner, H. Shtrikman, D. Mahalu, and U. Meirav, Phys. Rev. B **62**, 2188 (2000).
[12] B. H. Wu, J. C. Cao, and K-H. Ahn, Phys. Rev. B **72**, 165313 (2005).
[13] A.D. Güçlü, Q.-F. Sun, and H. Guo, Phys. Rev. B **68**, 245323 (2003).
[14] Y. Tanaka, N. Kawakami, Phys. Rev. B **72**, 085304 (2005).
[15] G.-H. Ding, C. K. Kim, K. Nahm, Phys. Rev. B **71**, 205313 (2005).
[16] D. Sztenkiel, R. Świrkowicz, J. Phys.: Condens. Matter **19**, 256205 (2007); J. Phys.: Condens. Matter **19**, 386224 (2007).
[17] G.-B. Zhang, S.-J. Wang, and L. Li, Phys. Rev. B **74**, 085106 (2006).
[18] R. López, R. Aguado, and G. Platero, Phys. Rev. Lett. **89**, 136802 (2002).
[19] C. A. Büsser, G. B. Martins, K. A. Al-Hassanieh, A. Moreo, and E. Dagotto, Phys. Rev. B **70**, 245303 (2004).
[20] J. S. Lim, M.-S. Choi, R. López, R. Aguado, Phys. Rev. B **74**, 205119 (2006).
[21] L. G. G. V. Dias da Silva, N. P. Sandler, K. Ingersent, and S. E. Ulloa, Phys. Rev. Lett. **97**, 096603 (2007).
[22] E. Vernek, N. Sandler, S. E. Ulloa, and E. V.Anda, Phys. E **34** (1-2), 608 (2006).
[23] T. Pohjola, H. Schoeller and G. Schön, Europhys. Lett., **54**, 241 (2001).
[24] Q.-F. Sun, and H. Guo, Phys. Rev. B **66**, 155308 (2002).
[25] T. Aono and M. Eto, Phys. Rev. B **63**, 125327 (2001).
[26] R. Aguado and D. C. Langreth, Phys. Rev. Lett. **85**, 1946 (2000).
[27] R. Aguado and D. C. Langreth, Phys. Rev. B **67**, 245307 (2003).
[28] Y. Tanaka, N. Kawakami, J. Phys. Soc. Jpn. **73**, 2795 (2004).
[29] T. Kuzmenko, K. Kikoin, Y. Avishai, Phys. Rev. B **69**, 195109 (2004); Phys. Rev. Lett. **96**, 046601 (2006).
[30] R. Žitko, J. Bonča, Phys. Rev. Lett. **98**, 047203
[31] Z.-T. Jiang, Q.-F. Sun, Y. Wang, Phys. Rev. B **72**, 045332 (2005).
[32] I. V. Dinu, M. Tolea, A. Aldea, Phys. Rev. B **76**, 113302 (2007).
[33] A. M. Lobos, A. A. Aligia, Phys. Rev. B **74**, 165417 (2006).
[34] F. Heidrich-Meisner, G. B. Martins, K. A. Al-Hassanieh, A. E. Feiguin, G. Chiappe, E.V. Anda, E. Dagotto, cond-mat/0705.1801. (2007).
[35] T. Tanamoto and Y. Nishi, Phys. Rev. B **76**, 155319 (2007); T. Tanamoto, Y. Nishi, and S. Fujita cond-math/0710.0912.
[36] A. Wysocki, J. Barnś, Acta Physicae Superficierum **9**, 177 (2006).
[37] P. Trocha, J. Barnaś, Phys. Rev. B **76**, 165432 (2007).
[38] P. Trocha, J. Barnaś, phys. stat. sol. (b) **244**, 2553 (2007).
[39] R. H. Dicke, Phys. Rev. **89**, 472 (1953).
[40] R. H. Dicke, Phys. Rev. **93**, 99 (1954).
[41] T. V. Shahbazyan and M. E. Raikh, Phys. Rev. B **49**, 17123 (1994).
[42] B. Wunsch and A. Chudnovsky, Phys. Rev. B **68**, 245317 (2003).
[43] P. A. Orellana, M. L. Ladrón de Guevara, and F. Claro, Phys. Rev. B **70**, 233315 (2004).
[44] P.A. Orellana, F. Dominguez-Adame, E. Diez, Physica E **35**,126 (2006).
[45] P. A. Orellana, G. A. Lara, and E. V. Anda, Phys. Rev. B **74**, 193315 (2006).
[46] T. Vorrath and T. Brandes, Phys. Rev. B **68**, 035309 (2003).
[47] T. Brandes and B. Kramer, Phys. Rev. Lett. **83**, 3021 (1999).
[48] T. Brandes, Phys. Rep. **408**, 315 (2005).
[49] P. Coleman, Phys. Rev. B **29**, 3036 (1984).
[50] P. Trocha, J. Barnaś, J. Phys.: Condens. Matter **20**, 125220 (2008).